Tissue Fraction Correction and Visual Analysis Increase Diagnostic Sensitivity in Predicting Malignancy of Ground-Glass Nodules on [^{18}F]-FDG PET/CT: A Bi-Centre Retrospective Study

Yun Hye Song
Hallym University Kangnam Sacred Heart Hospital https://orcid.org/0000-0002-0658-6474
Jung Won Moon
Hallym University Kangnam Sacred Heart Hostpital
Yoo Na Kim
Hallym University Kangnam Sacred Heart Hospital
Ji Young Woo
Hallym University Kangnam Sacred Heart Hospital
Hye Joo Son
Dankook University Hospital
Suk Hyun Lee (shlee0021@hallym.or.kr)
Hallym University Kangnam Sacred Heart Hostpital
Hee Sung Hwang
Hallym University Sacred Heart Hospital

Research Article

Keywords: ground-glass nodule, tissue fraction correction, visual analysis, [18F]-FDG positron-emission tomography/computed tomography

Posted Date: October 19th, 2021

DOI: https://doi.org/10.21203/rs.3.rs-976134/v1

Abstract

Purpose: We investigated the role of [^{18}F]-FDG positron-emission tomography/computed tomography (PET/CT) in evaluating ground-glass nodules (GGNs) by visual analysis and tissue fraction correction.

Methods: A total of 40 pathologically confirmed ≥1-cm GGNs were evaluated visually and semi-quantitatively. [^{18}F]-FDG uptake of GGN distinct from background lung activity was considered positive in visual analysis. In semi-quantitative analysis, we performed tissue fraction correction for the maximum standardised uptake value (SUV_{max}) of GGN.

Results: Of 40 GGNs, 25 (62.5%) were adenocarcinomas, 9 (22.5%) were minimally invasive adenocarcinomas (MIAs), and 6 (15%) were adenocarcinomas in situ (AIS). On visual analysis, adenocarcinoma showed the highest positivity rate among the three pathology groups (88.0%, 44.4%, 16.7%, respectively). Both SUV_{max} and tissue fraction corrected SUV_{max} (SUV_{maxTF}) were in order of adenocarcinoma > MIA > AIS (p = 0.033 and 0.018, respectively). SUV_{maxTF} was significantly higher than SUV_{max} before correction (2.4 [1.9–3.0] vs. 1.3 [0.8–1.8], p < 0.001). When using a cut-off value of 2.5, the positivity rate of GGNs was significantly higher in SUV_{maxTF} than in SUV_{max} (50.0% vs. 5.0%, p < 0.001).

Conclusions: Tissue fraction correction and visual analysis increased the diagnostic sensitivity of [^{18}F]-FDG PET/CT in predicting malignancy of lung GGN.

Introduction

With the development of thin section and high-resolution chest computed tomography (CT) [1-3], the detection rate of ground-glass nodules (GGN) has also been increasing. Lesions of various aetiologies can be seen as GGNs, representatively benign lesions such as inflammatory diseases, focal haemorrhages, fibroses and precancerous lesions, such as atypical adenomatous hyperplasia. Also, malignancies, such as adenocarcinoma in situ (AIS), minimally invasive adenocarcinoma (MIA), and some invasive adenocarcinomas have been reported as GGNs [4-6].

[^{18}F]-fluorodeoxyglucose (FDG) positron-emission tomography/computed tomography (PET/CT) is known to have high sensitivity and specificity in differentiating benign and malignant solid lung nodules [7-9]. Therefore, [^{18}F]-FDG] PET/CT is strongly recommended as a method to evaluate a single solid lung nodule according to the Fleischner Society 2017 Guidelines [10]. However, the role of [^{18}F]-FDG PET/CT in evaluating a subsolid nodule remains unclear [11-13].

Several studies have shown that non-small cell lung cancer (NSCLC) expressed as subsolid nodules has lower [^{18}F]-FDG uptake than other types of NSCLC. In particular, the false-negative rate of a malignant pure GGN has been reported as high as 90–100% [13-16]. One of the reasons for the low [^{18}F]-FDG uptake of malignant subsolid nodules is that [^{18}F]-FDG is not distributed in the air portion within the nodule, which may underestimate the [^{18}F]-FDG uptake of the solid portion.

Lambrou et al. presented a method to correct the air fraction of the lung by measuring the Hounsfield units (HUs) in interstitial lung disease. The air fraction may be heterogeneous depending on the severity of interstitial lung disease, so it was intended to correct this effect on [^{18}F]-FDG uptake [17]. If this method is applied to pure GGNs, it can be expected to measure the [^{18}F]-FDG uptake of the solid portion of the nodule, excluding the air fraction.

The study aim was to investigate the role of [^{18}F]-FDG PET/CT in evaluating GGNs and determine if tissue fraction correction is helpful for interpreting [^{18}F]-FDG uptake.

Materials And Methods

Subjects

This study was approved by the Institutional Review Board (IRB) of Kangnam Sacred Heart Hospital (IRB no. 2021-05-026) and Hallym Sacred Heart Hospital (IRB no. 2021-08-032). The IRB waived informed consent of this retrospective study. Among the patients with pure GGNs ≥ 1 cm on chest CT at Kangnam Sacred Heart Hospital from June 2012 to December 2020 and Hallym University Sacred Heart Hospital from November 2013 to December 2020, we analysed those who underwent [^{18}F]-FDG PET/CT within 90 days (Figure 1). The patient's age at diagnosis, sex, smoking history, date of chest CT, date of PET/CT, date and method of pathological confirmation, and final pathology were obtained from electronic medical records. The size and location of GGNs were obtained through chest CT. All patients were pathologically confirmed. Due to the slow-growing tendency of GGNs, their benign or malignant nature was not determined by imaging follow-up.

PET/CT imaging protocol

We acquired [^{18}F]-FDG PET/CT images under the following conditions. Before PET/CT, the patient fasted for >6 hours and was injected with 5.18 MBq/kg (0.14 mCi/kg) of [^{18}F]-FDG. The blood glucose level was controlled to be <8.33 mmol/L (150 mg/dL). PET/CT images were acquired approximately 60 minutes after [^{18}F]-FDG injection on a Gemini TF 16 PET/CT scanner (Philips Healthcare) and Gemini TF 64 PET/CT scanner (Philips Healthcare). After the initial low-dose CT (120 kVp, 50 mAs, 4-mm slice thickness) scan, PET images were obtained in 3D mode from the skull base to mid-thigh at 7–10 beds, 2 minutes each. The PET images were reconstructed by using the 3D row-action maximum likelihood algorithm and the iterative ordered subsets expectation maximisation algorithm (3 iterations, 33 subsets, no filtering), and CT-based attenuation correction was performed. Kangnam Sacred Heart Hospital and Hallym University Sacred Heart Hospital used PET/CT scanners with the same PET resolution and followed the same PET/CT imaging protocol.

PET/CT image analysis

Two experienced nuclear medicine board-certified physicians (S.H.L, H.J.S) performed visual analysis. The GGN was considered positive if there was [^{18}F]-FDG uptake distinct from background lung activity, otherwise, it was considered to be negative. If the results were discordant, the two physicians reviewed them together to reach a consensus.

For semi-quantitative analysis, the maximum standardised uptake value (SUV_{max}) was measured on a workstation (Advantage Workstation 4.7, GE Healthcare) by placing a volume of interest over each GGN. For tissue fraction correction of SUV_{max}, we made the following assumptions:

1) By adopting the method of Lambrou et al., the SUV of the solid portion within the GGN can be obtained by excluding the air fraction in which [^{18}F]-FDG is not distributed.

2) This study was conducted on pure GGNs only, and we assumed that the density within a GGN was homogeneous.

The formula for SUV_{max} correction by Lambrou et al. is as follows:

1) The tissue fraction of the GGN is k, and the air fraction is $(1 - k)$.

2) The HU of a GGN (HU_{GGN}) can be expressed as follows.

$$HU_{GGN} = k\,HU_{Tissue} + (1 - k)\,HU_{Air}$$

3) Converting to the expression for k, we get:

$$k = (HU_{GGN} - HU_{Air}) / (HU_{Tissue} - HU_{Air})$$

4) We assumed that the HU of the lung tissue fraction of the GGN would be similar to that of other solid organs, such as the liver, so we assigned a value of 50 to HU_{Tissue}. HU_{Air} is -1000. The HU_{GGN} of each GGN was measured on low-dose precontrast CT images of PET/CT because many patients had only enhanced chest CT images.

5) If SUV_{max} is divided by k, the tissue fraction corrected SUV_{max} (SUV_{maxTF}) excluding the air fraction can be obtained.

$$SUV_{maxTF} = SUV_{max} / k$$

We set the cut-off value of SUV_{max} and SUV_{maxTF} to 2.5, which is commonly used [18].

Statistical analysis

The Kruskal–Wallis test was performed for age at diagnosis, the interval between chest CT and PET/CT, the interval between PET/CT and pathological confirmation, GGNs size, HU, SUV_{max} and SUV_{maxTF} of the nodule. Fisher's exact test was performed for the patient's sex, smoking history, pathological confirmation

method, percentage of nodules with SUV_{max} and SUV_{maxTF} > 2.5, and the visual positivity rate in each pathological group. The Wilcoxon signed-rank test was performed to determine the significance of changes in SUV_{max} when tissue fraction correction was performed in each pathology group. The McNemar test was performed to see if the number of GGNs with an SUV_{max} of ≥ 2.5 showed a significant increase when tissue fraction correction was performed. A *p*-value of <0.05 was considered to be indicative of statistical significance. Statistical analyses were performed by using IBM SPSS Statistics for Windows (Version 27., IBM Corp. Armonk, NY, USA) and VassarStats (http://www.vassarstats.net). The post-hoc test was performed with Bonferroni correction.

Results

A total of 38 patients were enrolled at Hallym University Sacred Heart Hospital (n = 29), Kangnam Sacred Heart Hospital (n = 9), and a total of 40 GGNs (36 patients with one GGN, two patients with two GGNs) were classified according to their pathology. Of the total 40 GGNs, 25 were adenocarcinomas, 9 were MIAs and 6 were AISs. Among these pathology groups, there were no significant differences in age, sex, smoking history, nodule size, HU, the interval between chest CT and [^{18}F]-FDG PET/CT, the interval between [^{18}F]-FDG PET/CT and pathological confirmation, and pathological confirmation method (Table 1).

Table 1
Patients' characteristics

Characteristics	***n* = 38**
Age at diagnosis, year, median (Q1 –Q3)	64.0 (59.0 –68.0)
Sex	
Male, *n* (%)	13 (34.2%)
Female, *n* (%)	25 (65.8%)
Smoking history	
Current smoker, *n* (%)	3 (7.9%)
Former smoker, *n* (%)	0 (0.0%)
Non-smoker, *n* (%)	35 (92.1%)
Reason for [^{18}F]-FDG PET/CT	
For ground-glass nodule evaluation	35 (92.1%)
For other malignancy evaluation	3 (7.9%)
Interval between CT and [^{18}F]-FDG PET/CT, days, median (Q1 –Q3)	17.5 (11.5 –24.8)
Interval between [^{18}F]-FDG PET/CT and biopsy, days, median (Q1 –Q3)	5.0 (2.0 –10.5)
Q1, 25th percentile; Q3, 75th percentile	

The chest CT and [^{18}F]-FDG PET/CT characteristics in each pathology group are shown in Table 2. In visual analysis, the positivity rate was 88.0% (highest) for adenocarcinoma, 44.4% for MIA, and 16.7% (lowest) for AIS. In the post-hoc test, there was a significant difference in positivity rates between adenocarcinoma and AIS ($p = 0.002$). Both before and after tissue fraction correction, the SUV_{max} values were in the order of adenocarcinoma > MIA >AIS, with a significant difference between adenocarcinoma and AIS ($p = 0.012$, $p = 0.008$, respectively). After tissue fraction correction, the median SUV_{max} was increased by 84.6% ($p < 0.001$), and the positivity rate of [^{18}F]-FDG PET/CT, with an SUV_{max} cut-off value of 2.5, also increased significantly from 5.0–50.0% ($p < 0.001$). Representative cases are shown in Figures 2 and 3.

Table 2

Characteristics of the chest CT and [^{18}F]-FDG PET/CT findings

Characteristics	Adenocarcinoma (*n* = 25)	MIA (*n* = 9)	AIS (*n* = 6)	Total (*n* = 40)	*p*
Size of nodule, mm, median (Q1–Q3)	19.0 (15.0–23.0)	13.3 (10.0–20.0)	14.7 (12.0–16.8)	16.8 (12.0–23.0)	0.125
Hounsfield unit, median (Q1–Q3)	−436.6 (−528.5 to −377.0)	−410.5 (−630.5 to −313.0)	−576.9 (−630.5 to −435.2)	−437.2 (−598.4 to −378.5)	0.406
Method for pathological confirmation					0.227
Needle biopsy, *n* (%)	7 (28.0%)	0 (0.0%)	1 (16.7%)	8 (20.0%)	
Surgical confirmation, *n* (%)	18 (72.0%)	9 (100.0%)	5 (83.3%)	32 (80.0%)	
Location					N/A
Right upper lobe, *n* (%)	9 (36.0%)	3 (33.3%)	4 (66.7%)	16 (40.0%)	
Right middle lobe, *n* (%)	0 (0.0%)	3 (33.3%)	1 (16.7%)	4 (10.0%)	
Right lower lobe, *n* (%)	3 (12.0%)	0 (0.0%)	0 (0.0%)	3 (7.5%)	
Left upper lobe, *n* (%)	6 (24.0%)	2 (22.1%)	0 (0.0%)	8 (20.0%)	
Left lower lobe, *n* (%)	7 (28.0%)	1 (11.1%)	1 (16.7%)	9 (22.5%)	
Histological subtype					N/A
Lepidic predominant, *n* (%)	16 (64%)	9 (100.0%)	3 (50.0%)	28 (70.0%)	
Acinar predominant, *n* (%)	4 (16%)	0 (0.0%)	0 (0.0%)	4 (10.0%)	
Mixed lepidic and acinar, *n* (%)	3 (12%)	0 (0.0%)	0 (0.0%)	3 (7.5%)	
Papillary predominant, *n* (%)	1 (4%)	0 (0.0%)	0 (0.0%)	1 (2.5%)	
Unconfirmed, *n* (%)	1 (4%)	0 (0.0%)	3 (50.0%)	4 (10.0%)	

AIS, adenocarcinoma in situ; MIA, minimally invasive adenocarcinoma; Q1, 25th percentile; Q3, 75th percentile; SUV_{max}, maximum standardised uptake value; SUV_{maxTF}, tissue fraction corrected SUV_{max}

*$P < 0.05$ was considered statistically significant.

Characteristics	Adenocarcinoma (*n* = 25)	MIA (*n* = 9)	AIS (*n* = 6)	Total (*n* = 40)	*p*
Visual analysis of [^{18}F]-FDG PET/CT					0.001*
Positive, *n* (%)	22 (88.0%)	4 (44.4%)	1 (16.7%)	27 (67.5%)	
Semiquantitative analysis of [^{18}F]-FDG PET/CT					
SUV_{max}, median (Q1–Q3)	1.3 (1.1-1.8)	1.1 (0.7-1.8)	0.6 (0.5-0.9)	1.3 (0.8-1.8)	0.033*
SUV_{maxTF}, median (Q1–Q3)	2.6 (2.2-3.1)	2.2 (1.9-2.9)	1.6 (1.5-1.7)	2.4 (1.9-3.0)	0.018*
$SUV_{max} \geq 2.5$, *n* (%)	2 (8.0%)	0 (0.0%)	0 (0.0%)	2 (5.0%)	0.990
$SUV_{maxTF} \geq 2.5$, *n* (%)	15 (60.0%)	4 (44.4%)	1 (16.7%)	20 (50.0%)	0.195

AIS, adenocarcinoma in situ; MIA, minimally invasive adenocarcinoma; Q1, 25th percentile; Q3, 75th percentile; SUV_{max}, maximum standardised uptake value; SUV_{maxTF}, tissue fraction corrected SUV_{max}

*$P < 0.05$ was considered statistically significant.

Discussion

This appears to be the first study to attempt evaluating [^{18}F]-FDG uptake by correcting tissue fraction in malignant pure GGNs. Tissue fraction correction was first introduced by Lambrou et al. to exclude the effect of heterogeneous density in measuring lung [^{18}F]-FDG uptake in patients with interstitial lung disease [17]. We thought that FDG uptake, excluding the air fraction of GGN, could be measured by applying Lambrou's method because GGNs contain a high air fraction, and the density varies among GGNs. However, it was not known which value was appropriate to apply to HU_{Tissue} in the formula. However, we assumed that the tissue fraction constituting GGN would have a similar density to that of other solid organs, such as the liver, so we applied 50 as done by Bondue et al. [19]. As we expected, when this method was applied, SUV_{maxTF} increased the sensitivity of detecting a malignant pure GGN, and adenocarcinoma expressed as GGNs showed high sensitivity on both visual analysis (88.0%) and semi-quantitative analysis after tissue fraction correction (60.0%).

The pure GGNs enrolled in this study were confirmed to be adenocarcinoma, MIA and AIS in pathological analysis. Travis et al. reclassified lung adenocarcinoma in 2011. AIS, formerly called bronchioloalveolar carcinoma, is a small localised adenocarcinoma of <3 cm characterised by lepidic growth along with the alveolar structure. If a nodule has papillary, micropapillary, solid growth pattern, or infiltration into myofibroblastic stroma with an invasion of <5 mm, it is classified as an MIA. If there is an invasion of >5

mm, invasion of lymphatics, blood vessels, pleura or presence of tumour necrosis, the nodule is classified as an invasive adenocarcinoma [20]. Therefore, the invasiveness is in the order of adenocarcinoma > MIA > AIS. Similarly, our study showed [^{18}F]-FDG positivity, SUV_{max}, and SUV_{maxTF} for each in the order of adenocarcinoma > MIA > AIS. Therefore, we think that [^{18}F]-FDG PET/CT reflects the histological invasiveness of GGN.

In other studies, the false negativity rate of malignant pure GGN has been reported as high as 90–100% [13-16], which is thought to be because of the high proportion of <1-cm nodules [13, 21] or the strict criterion of [^{18}F]-FDG uptake positivity (a $SUV_{max} \geq 2.5$ [14] or a higher [^{18}F]-FDG uptake than that of mediastinal blood pool activity [15]). To avoid high false negativity rates due to small size or a high standard of positive criteria, we evaluated only pure >1-cm GGNs and set the positivity criteria to be [^{18}F]-FDG uptake higher than background lung activity in visual analysis. As a result, the positivity rate of visual analysis was 67.5% (88.0% for adenocarcinoma), whereas the positivity rate was very low at 5%, as in other studies when the SUV_{max} 2.5 was set as the cut-off. When the tissue fraction was corrected, the sensitivity increased by 50.0% (60.0% for adenocarcinoma) despite that a high SUV_{max} cut-off of 2.5 was applied, which is higher than previous studies.

Vesselle et al. reported different mean SUV_{max} values according to the histology of lung cancer (large cell, 12.6 ± 5.5; squamous, 11.7 ± 4.5; adenocarcinoma, 9.2 ± 5.8; bronchioloalveolar carcinoma, 3.2 ± 1.7) [22]. In our study, invasive adenocarcinoma showed a relatively low SUV_{max} after the tissue fraction correction (mean SUV_{maxTF} = 3.2 ± 2.4). According to Yoshizawa et al., among the subtypes of invasive adenocarcinoma divided by their growth patterns, solid- and micropapillary type adenocarcinomas showed poor prognosis, with a 5-year disease-free survival of 67–76%. On the other hand, acinar, papillary, and lepidic types showed 5-year disease-free survivals ranging from 83–90%, with intermediate clinical behaviour [23]. These growth patterns are known as stage-independent prognostic indicators [24], and Moon et al. reported that no micropapillary or solid components were found in pure GGNs [25]. In our study, in 36 GGNs with confirmed histological subtypes out of 40 GGNs, the most common lepidic predominant type was 70%, followed by acinar predominant, mixed lepidic and acinar and papillary types. Only two GGNs contained a tiny proportion of micropapillary type (<5% of cancer lesions). Not a single GGN showed a solid component. Due to these differences in histological subtypes, the SUV_{max} may have been lower than solid lung cancer even with tissue fraction correction. In addition, it is well known that the growth rate is lower for GGNs than solid nodules or mixed GGNs. According to Hasegawa et al., the median volume doubling time of pure GGNs is about 831 days, which is much longer than that for mixed GGNs (about 457 days), suggesting that pure GGNs are relatively indolent [26]. Slow-growing tumours are thought to have a low metabolic demand because of a low number of metabolically active malignant cells [11, 27], which may also be one of the reasons why the SUV_{max} was low even after the tissue fraction was corrected.

McDermott et al. reported that the mean SUV_{max} of 21 malignant GGNs was 0.8 ± 0.3, which is even lower than that of 106 benign GGNs (1.6 ± 1.5, p = 0.002) [28]; however, malignant GGNs showed a mean

SUV_{max} of 1.5 ± 1.2 in our study, which is significantly higher than in their study (p = 0.011). We performed a biopsy on all 40 malignant GGNs, whereas McDermott et al. performed biopsy confirmation on only 3 out of 127 GGNs. Consequently, it is difficult to understand the discrepancy between the two studies clearly. If McDermott et al. included many malignant GGNs with low [^{18}F]-FDG uptakes, such as AIS and MIA, it is possible to show such low [^{18}F]-FDG uptake of malignant GGNs.

In general, CT attenuation, presenting as GGNs, is known to be higher for invasive adenocarcinoma than for the precursor [29, 30]. Recent studies have reported that the SUV_{max} positively correlates with the size, cellularity, and aggressiveness of the lesion but negatively correlates with the percentage of ground-glass opacity [20, 23, 27, 31-33]. In our study, there was no significant difference in HUs between the three pathology groups, but significant differences were found in the SUV_{max} and SUV_{maxTF}. Thus, [^{18}F]-FDG PET/CT may be more helpful in analysing GGNs than HU.

This study had several limitations. First, there was no benign lesion among the GGNs included in this study, so specificity could not be calculated. Due to the slow-growing nature of GGNs, it was hard to determine whether or not a nodule was benign by imaging follow-up. Second, respiratory gating was not performed. If misregistration occurred, we then performed visual analysis and semi-quantitative analysis, assuming that the visually discernible [^{18}F]-FDG uptake near the GGN was the [^{18}F]-FDG uptake of the GGN. However, [^{18}F]-FDG uptake could have been underestimated due to inaccurate attenuation correction.

Conclusions

Tissue fraction correction and visual analysis increased the sensitivity of predicting the malignancy of pure GGNs on [^{18}F]-FDG PET/CT.

Declarations

Acknowledgements

This research was not funded by any organisation. The authors would like to thank Enago (http://www.enago.co.kr) for the English language review.

Author Contributions

The authors' contributions are as follows: YH Song participated in the study design, drafting of the manuscript, and data acquisition and analysis, JW Moon, YN Kim, JY Woo, and HJ Son participated in data acquisition and data analysis, HJ SON participated in data analysis, SH Lee and HS Hwang participated in the study conception and design, data analysis, manuscript revision, and approval of the final content of the manuscript. All authors have read and approved the final manuscript.

Data Availability

The datasets analysed during the current study are available from the corresponding author on reasonable request.

Competing Interests

The authors declare that they have no conflict of interest.

Informed consent

The institutional review board approved this study and waived informed consent for the retrospective study.

Ethics approval

All procedures performed in studies involving human participants were in accordance with the ethical standards of the institutional and national research committee and with the 1964 Helsinki declaration and its later amendments or comparable ethical standards.

References

1. Niu R, Shao X, Shao X, Wang J, Jiang Z, Wang Y. Lung adenocarcinoma manifesting as ground-glass opacity nodules 3 cm or smaller: Evaluation with combined high-resolution CT and PET/CT Modality. AJR Am J Roentgenol. 2019,213:W236-W45. https://doi.org/10.2214/AJR.19.21382.
2. Goo JM, Park CM, Lee HJ. Ground-glass nodules on chest CT as imaging biomarkers in the management of lung adenocarcinoma. AJR Am J Roentgenol. 2011,196:533-43. https://doi.org/10.2214/AJR.10.5813.
3. Zhuo Y, Shan F, Yang S, Zhan Y, Shi Y, Zhang Z. Advances in differential diagnosis of pulmonary ground glass opacity on high resolution computed tomography and histopathology. Radiol Infect Dis. 2020,7:7-11. https://doi.org/10.1016/j.jrid.2020.03.003.
4. Chang Min Park M, Jin Mo GOO, MD, Hyun Ju Lee, MD, Chang Hyun Lee, MD, Eun Ju Chun, MD, Jung-Gi Im, MD. Nodular ground-glass opacity at thin-section CT: Histologic correlation and evaluation of change at follow-up. RadioGraphics. 2007,27:391-408.
5. Hyun Ju Lee M, et al. Nodular ground-glass opacities on thin-section CT: Size change during follow-up and pathological results. Korean J Radiol. 2007,8.
6. Nakata M, Saeki H, Takata I, Segawa Y, Mogami H, Mandai K, et al. Focal ground-glass opacity detected by low-dose helical CT. Chest. 2002,121:1464-7. https://doi.org/10.1378/chest.121.5.1464.
7. Christensen JA, Nathan MA, Mullan BP, Hartman TE, Swensen SJ, Lowe VJ. Characterisation of the solitary pulmonary nodule: 18F-FDG PET versus nodule-enhancement CT. AJR Am J Roentgenol. 2006,187:1361-7. https://doi.org/10.2214/AJR.05.1166.
8. Michael K. Gould M, MS, Courtney C. Maclean, BA, Ware G. Kuschner, MD, Chara E. Rydzak, BA, Douglas K. Owens, MD, MS. Accuracy of positron emission tomography for diagnosis of pulmonary

nodules and mass lesions: a meta-analysis. JAMA. 2001,285:914-24.

9. Val J. Lowe ea. Prospective investigation of positron emission tomography in lung nodules. J Clin Oncol. 1998,16.
10. MacMahon H, Naidich DP, Goo JM, Lee KS, Leung ANC, Mayo JR, et al. Guidelines for Management of incidental pulmonary nodules detected on CT images: From the Fleischner Society 2017. Radiology. 2017,284:228-43. https://doi.org/10.1148/radiol.2017161659.
11. Heyneman LE, Patz, E.F. PET imaging in patients with bronchioloalveolar cell carcinoma. Lung Cancer. 2002,38:261-6.
12. Higashi K, Ueda Y, Seki H, Yuasa K, Oguchi M, Noguchi T, et al. Fluorine-18-FDG PET imaging is negative in bronchioloalveolar lung carcinoma. J Nucl Med. 1998,39:1016-20.
13. Hu L, Pan Y, Zhou Z, Gao J. Application of positron emission tomography-computed tomography in the diagnosis of pulmonary ground-glass nodules. Exp Ther Med. 2017,14:5109-13. https://doi.org/10.3892/etm.2017.5194.
14. Nishii K, Bessho A, Fukamatsu N, Ogata Y, Hosokawa S, Sakugawa M, et al. Statistical analysis of (18)F-fluorodeoxyglucose positron-emission tomography/computed tomography ground-glass nodule findings. Mol Clin Oncol. 2018,9:279-82. https://doi.org/10.3892/mco.2018.1670.
15. Wu HB, Wang L, Wang QS, Han YJ, Li HS, Zhou WL, et al. Adenocarcinoma with BAC features presented as the nonsolid nodule is prone to be false-negative on 18F-FDG PET/CT. Biomed Res Int. 2015,2015:243681. https://doi.org/10.1155/2015/243681.
16. Nomori H, Watanabe K, Ohtsuka T, Naruke T, Suemasu K, Uno K. Evaluation of F-18 fluorodeoxyglucose (FDG) PET scanning for pulmonary nodules less than 3 cm in diameter, with special reference to the CT images. Lung Cancer. 2004,45:19-27. https://doi.org/10.1016/j.lungcan.2004.01.009.
17. Lambrou T, Groves AM, Erlandsson K, Screaton N, Endozo R, Win T, et al. The importance of correction for tissue fraction effects in lung PET: preliminary findings. Eur J Nucl Med Mol Imaging. 2011,38:2238-46. https://doi.org/10.1007/s00259-011-1906-x.
18. Coleman RE. PET in lung cancer. J Nucl Med. 1999,40:814-20.
19. Bondue B, Castiaux A, Van Simaeys G, Mathey C, Sherer F, Egrise D, et al. Absence of early metabolic response assessed by 18F-FDG PET/CT after initiation of antifibrotic drugs in IPF patients. Respir Res. 2019,20:10. https://doi.org/10.1186/s12931-019-0974-5.
20. William D. Travis M, et al. International Association for the Study of Lung Cancer/American Thoracic Society/European Respiratory Society International Multidisciplinary Classification of Lung Adenocarcinoma. J Thorac Oncol. 2011,6.
21. Evangelista L, Panunzio A, Scagliori E, Sartori P. Ground glass pulmonary nodules: their significance in oncology patients and the role of computer tomography and 18F-fluorodeoxyglucose positron emission tomography. Eur J Hybrid Imaging. 2018,2:2. https://doi.org/10.1186/s41824-017-0021-z.
22. Vesselle H, Salskov A, Turcotte E, Wiens L, Schmidt R, Jordan CD, et al. Relationship between non-small cell lung cancer FDG uptake at PET, tumor histology, and Ki-67 proliferation index. J Thorac

Oncol. 2008,3:971-8. https://doi.org/10.1097/JTO.0b013e31818307a7.

23. Yoshizawa A, Motoi N, Riely GJ, Sima CS, Gerald WL, Kris MG, et al. Impact of proposed IASLC/ATS/ERS classification of lung adenocarcinoma: prognostic subgroups and implications for further revision of staging based on analysis of 514 stage I cases. Mod Pathol. 2011,24:653-64. https://doi.org/10.1038/modpathol.2010.232.
24. Warth A, Muley T, Meister M, Stenzinger A, Thomas M, Schirmacher P, et al. The novel histologic International Association for the Study of Lung Cancer/American Thoracic Society/European Respiratory Society classification system of lung adenocarcinoma is a stage-independent predictor of survival. J Clin Oncol. 2012,30:1438-46. https://doi.org/10.1200/JCO.2011.37.2185.
25. Moon Y, Lee KY, Park JK. The prognosis of invasive adenocarcinoma presenting as ground-glass opacity on chest computed tomography after sublobar resection. J Thorac Dis. 2017,9:3782-92. https://doi.org/10.21037/jtd.2017.09.40.
26. M Hasegawa M, S Sone, MD, S Takashima, MD, F LI, MD, Z-G Yang, MD, Y Maruyama, MD, and T Watanabe, MD. Growth rate of small lung cancers detected on mass CT screening. Brit J Radiol. 2000,73:1252-9.
27. Goudarzi B, Jacene HA, Wahl RL. Diagnosis and differentiation of bronchioloalveolar carcinoma from adenocarcinoma with bronchioloalveolar components with metabolic and anatomic characteristics using PET/CT. J Nucl Med. 2008,49:1585-92. https://doi.org/10.2967/jnumed.108.052712.
28. McDermott S, Kilcoyne A, Wang Y, Scott JA, Halpern EF, Ackman JB. Comparison of the (18)F-FDG avidity at PET of benign and malignant pure ground-glass opacities: a paradox? Clin Radiol. 2019,74:187-95. https://doi.org/10.1016/j.crad.2018.12.009.
29. Ikeda K, Awai K, Mori T, Kawanaka K, Yamashita Y, Nomori H. Differential diagnosis of ground-glass opacity nodules: CT number analysis by three-dimensional computerised quantification. Chest. 2007,132:984-90. https://doi.org/10.1378/chest.07-0793.
30. Qi L, Xue K, Li C, He W, Mao D, Xiao L, et al. Analysis of CT morphologic features and attenuation for differentiating among transient lesions, atypical adenomatous hyperplasia, adenocarcinoma in situ, minimally invasive and invasive adenocarcinoma presenting as pure ground-glass nodules. Sci Rep. 2019,9:14586. https://doi.org/10.1038/s41598-019-50989-1.
31. Kim TJ, Park CM, Goo JM, Lee KW. Is there a role for FDG PET in the management of lung cancer manifesting predominantly as ground-glass opacity? AJR Am J Roentgenol. 2012,198:83-8. https://doi.org/10.2214/AJR.11.6862.
32. Shao X, Niu R, Jiang Z, Shao X, Wang Y. Role of PET/CT in management of early lung adenocarcinoma. AJR Am J Roentgenol. 2020,214:437-45. https://doi.org/10.2214/AJR.19.21585.
33. Kim KH, Ryu SY, Lee HY, Choi JY, Kwon OJ, Kim HK, et al. Evaluating the tumor biology of lung adenocarcinoma: A multimodal analysis. Medicine (Baltimore). 2019,98:e16313. https://doi.org/10.1097/MD.0000000000016313.

Figures

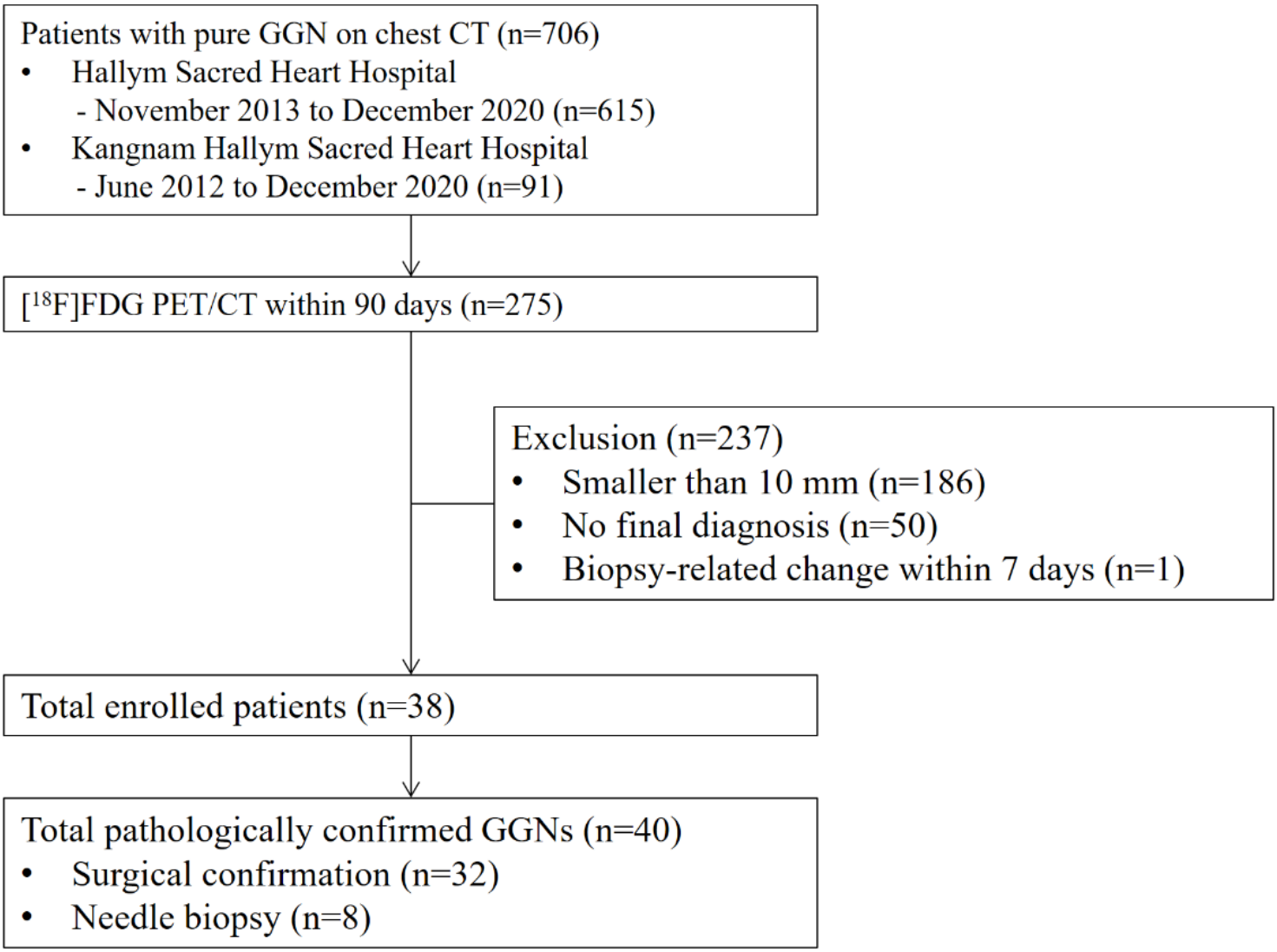

Figure 1

Flow diagram of patient enrolment

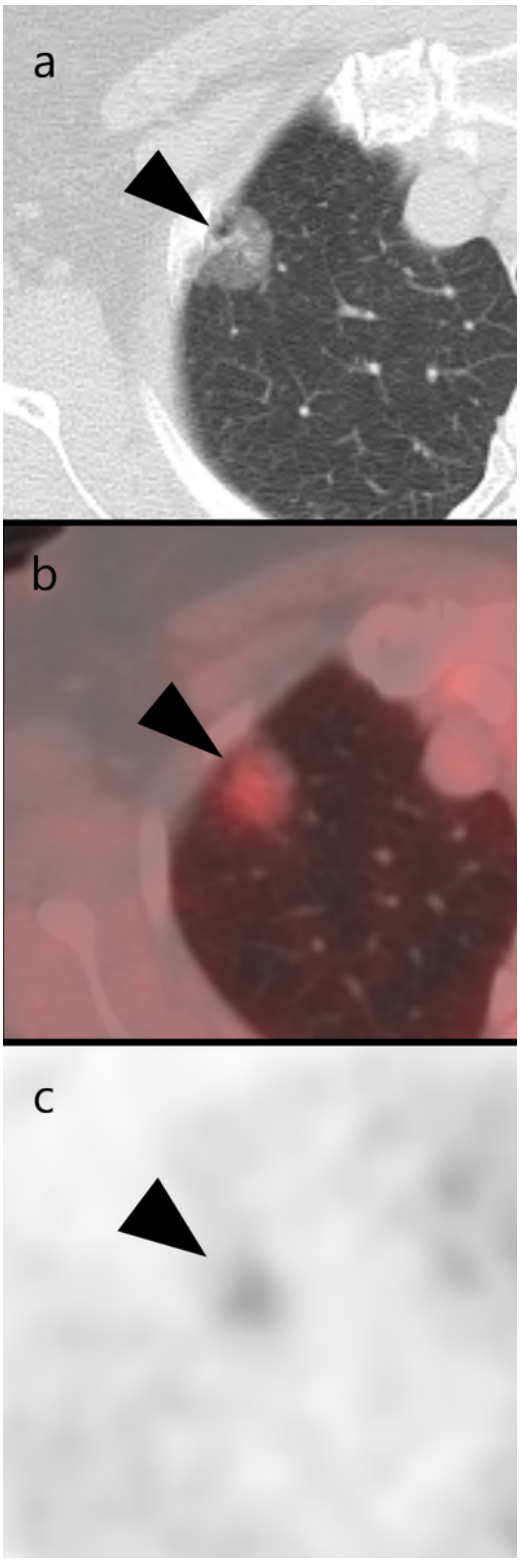

Figure 2

Example of adenocarcinoma A 58-year-old woman with a 20-mm ground-glass nodule shown on chest CT (a) with visually positive [18F]-FDG uptake (b, c). The HU of the nodule is −436, and the SUVmax increased from 1.99 to 3.70 after tissue fraction correction, which is higher than the cut-off value of 2.50. The nodule is diagnosed as adenocarcinoma after surgery

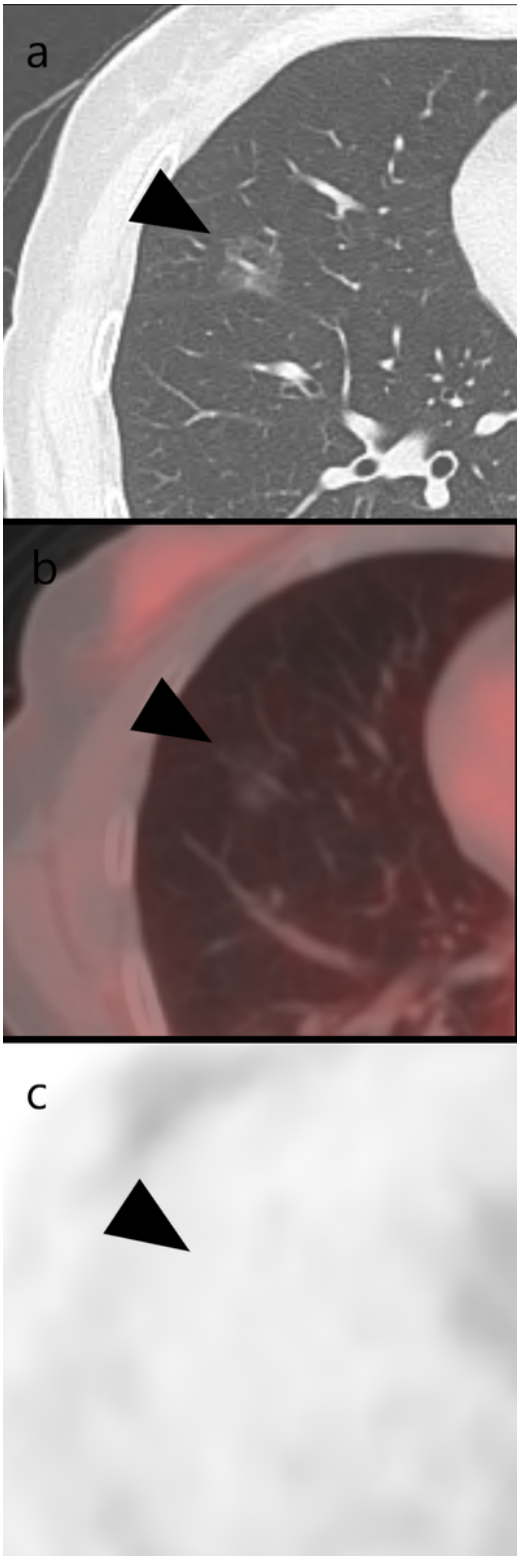

Figure 3

Example of adenocarcinoma in situ A 60-year-old woman with a 17-mm ground-glass nodule shown on chest CT (a) with visually negative [18F]-FDG uptake (b, c). The HU of the nodule is −644, and the SUVmax increased from 0.52 to 1.53 after tissue fraction correction, which is lower than the cut-off value of 2.50. The nodule is diagnosed as adenocarcinoma in situ after surgery